Reflectivity of laser-produced plasmas generated by a high intensity ultrashort pulse*

R. Sauerbrey, J. Fure, S. P. Le Blanc, B. van Wonterghem, U. Teubner, and F. P. Schäfer

Citation: Physics of Plasmas **1**, 1635 (1994); doi: 10.1063/1.870665
View online: http://dx.doi.org/10.1063/1.870665
View Table of Contents: http://scitation.aip.org/content/aip/journal/pop/1/5?ver=pdfcov
Published by the AIP Publishing

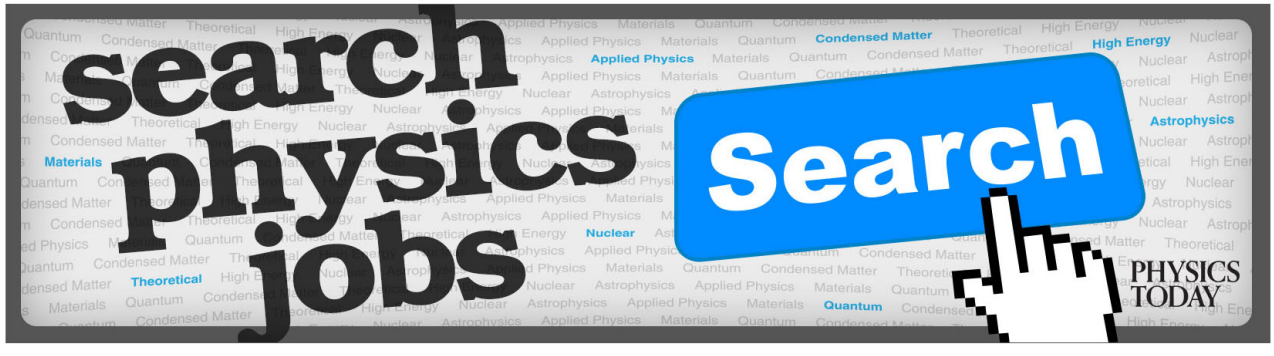

Reflectivity of laser-produced plasmas generated by a high intensity ultrashort pulse*

R. Sauerbrey,[†,a)] J. Fure, and S. P. Le Blanc
Rice Quantum Institute and Department of Electrical & Computer Engineering, Rice University, P.O. Box 1892, Houston, Texas 77251-1892

B. van Wonterghem, U. Teubner, and F. P. Schäfer
Abteilung Laserphysik, Max-Planck-Institut für Biophysikalische Chemie, Postfach 2841, Am Fassberg, D-3400 Gottingen, Germany

(Received 5 November 1993; accepted 3 January 1994)

Solid state density aluminum and carbon plasmas were generated by 350 fs KrF laser pulses at intensities of 10^{17} W cm^{-2}. Reflectivity, x-ray emission, and spectra of the backscattered radiation were measured as a function of the laser polarization, angle of incidence, and intensity (I). For p-polarized light, the absorption (A) is almost intensity independent for 10^{15} W cm$^{-2} < I < 2\times 10^{17}$ W cm^{-2}, and can reach values up to $A=0.8$. For constant laser intensity, p-polarized light is up to a factor of 15 more efficient in generating x rays than s-polarized light. A polarization and angle of incidence-dependent absorption mechanism, such as resonance absorption or vacuum heating, is consequently important. The spectral line shape and positions of the reflected radiation from the carbon plasma showed a substantial intensity dependence. It is demonstrated that the backscattered spectrum is influenced by the plasma expansion (Doppler effect) and the temporal development of the electron density.

I. INTRODUCTION

The recent development of high intensity ultrashort pulse lasers opens the possibility of generating solid density plasmas. It has been demonstrated that solid targets irradiated by high intensity laser pulses with pulse durations below 1 ps emit a broad x-ray spectrum that ranges from sub-keV energies to several MeV.[1–4] X-ray streak camera measurements[5,6] indicate picosecond and possibly even subpicosecond pulse durations for certain spectral components. For the practical use of such short pulse x-ray sources in biology, crystallography, microscopy, or solid state physics, efficient absorption of the laser radiation in the target, and a high conversion efficiency to x rays are important.

To characterize femtosecond laser-produced plasmas, several experiments and numerical simulations[5–13] of the properties of such plasmas have been conducted. To date, these investigations have examined the reflectivity as a function of several variables: the angle of incidence of the laser pulse, the characteristic scale length of the plasma, the electron ion collision frequency, and the electron density profile. Models that treat the reflectivity of the plasma as a constant can be used to infer effective scale lengths and collisionalities from the angular and polarization dependence of the reflectivity. However, such models and experimental measurements are insensitive to dynamic effects that may change the spectral shape of the reflected laser light through phase modulation. Thus, time-dependent modeling of the plasma and its reflectivity is necessary in order to interpret experimental results involving changes in the spectral line shape. At incident laser intensities of 10^{12} W cm^{-2}–10^{15} W cm^{-2}, Milchberg *et al.*[14] investigated spectral changes of backscattered laser pulses, and concluded that the spectral changes could be attributed to Doppler shifts. Umstadter *et al.*[15] have performed simulations of the evolution of a plasma profile by balancing ponderomotive forces and thermal pressure, and have shown that radiation pressure may significantly alter the evolution of a plasma profile, even for intensities $\sim 10^{15}$ W cm^{-2}. In the present experiments, with intensities up to 10^{17} W cm^{-2}, the optical properties of the plasma change rapidly and lead to phase modulation effects on the reflected spectra in addition to Doppler shifts.

In this paper we report on experiments that investigate the absorption of laser radiation, the spectra of the backscattered laser radiation, and the production of x rays in aluminum and carbon plasmas as a function of the angle of incidence, laser intensity, and polarization. A model that describes the time dependence of the electron density and the plasma scale length is developed to characterize the evolution of the expanding plasma profile. The time-dependent plasma parameters are obtained by comparing the calculated backscattered laser spectra to the experimentally measured spectra.

II. EXPERIMENTS

High-density laser-produced plasmas were generated using the experimental setup shown in Fig. 1. Polished aluminum and glassy carbon targets[16] were irradiated by the focused beam of a subpicosecond KrF excimer laser. The KrF laser pulses were generated by amplifying the frequency doubled output from a subpicosecond distributed feedback dye laser (DFDL) in a conventional dis-

*Paper 9I1, Bull. Am. Phys. Soc. **38**, 2098 (1993).
†Invited speaker.
a)Present address: Institut für Optik und Quantenelektronik Friedrich-Schiller Universität Jena, Max-Wien Platz 1, D-07743 Jena, Germany.

 1070-664X/94/1(5)/1635/8/$6.00

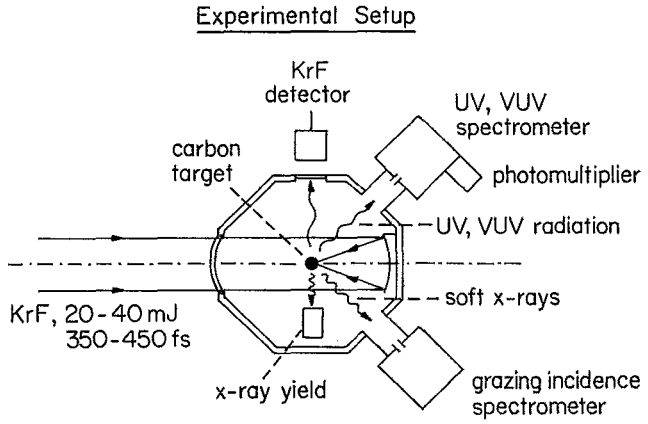

FIG. 1. Schematic of the experimental setup containing the target chamber and diagnostic equipment.

charge pumped excimer laser, followed by an x-ray preionized large aperture KrF laser, both operated at a repetition frequency of 1 Hz.[17,18] With this system, a short pulse energy output of about $E=30$ mJ was achieved in a 50 mm diam beam. The shot to shot energy fluctuation was typically less than 20%. The pulse duration of the amplified KrF laser pulse was measured by a multiple shot autocorrelator based on two photon ionization of NO to be (350 ± 50) fs.[17] The beam was focused by a $f/8$ Maksutov optics consisting of a thin meniscus lens and a spherical mirror onto the target. The polarization of the KrF laser could be changed by varying the polarization of the seed pulse injected into the amplifier, and was either in the s or p direction with respect to the target surface. The degree of polarization exceeded 95% at the entrance window of the target chamber.

It was found in previous experiments that a low intensity long pulse background superimposed on the subpicosecond laser pulse severely influences the laser plasma interaction.[5,9,19–24] It is therefore of the utmost importance to keep prepulses and pedestals caused by amplified spontaneous emission (ASE) in the excimer amplifiers at an intensity level well below the plasma production threshold on the target surface. In the present experiments a high contrast ratio was achieved by spatial separation of the amplifiers, repeated spatial filtering of the laser beam, and a reduction of the ASE levels in the amplifiers by using lean laser gas mixtures. The first discharge pumped amplifier was operated at a small signal single pass gain value of slightly below 1000 and a saturated amplification of about 150. For the large aperture amplifier the corresponding values were 300 and 30.

The single shot focal structure of the individual ASE components and focused femtosecond laser pulse was investigated by a three lens CaF_2 microscope (90× magnification) viewed through a CCD camera. The ASE of the final amplifier of about 1 mJ was found in a diffuse spot of about 2 mm diam, corresponding to an intensity of less than 2×10^6 W cm^{-2}. The ASE originating from the first amplifier reached a value of up to 0.5 mJ after amplification in the large aperture amplifier, and was focused to a spot of 300 μm diam on the target. This corresponds to an upper limit for the ASE intensity of $I_{ASE}\leqslant 4\times10^7$ W cm^{-2}. The 350 fs pulse was focused to an Airy-pattern-like structure with 60% of the energy in the central peak with a full width half-maximum (FWHM) diameter of (3.2±0.4) μm. For the maximum energy of $E=30$ mJ, this yields $I_{max}=6\times10^{17}$ W cm^{-2}. Consequently, for the intensity contrast ratio we obtain $I_{max}/I_{ASE}>1.5\times10^{10}$. The laser pulses were continuously attenuated by two thin dielectrically coated MgF_2 plates that were placed in the amplified beam under varying directions under conservation of the high contrast ratio. Due to a different amplifier arrangement for the aluminum experiment, the beam size was smaller, effectively giving a higher f number for the focusing optics. The diffraction limited limited spot size was (7.0±0.5) μm and the pulse width of the laser was 400 fs. The ASE was still focused in a different plane than the laser pulse, so the high contrast ratio between the laser pulse and the ASE was conserved.

The target was in the center of a vacuum chamber at a pressure of about 10^{-5} Torr and was scanned to provide a fresh spot for each laser shot. The glassy carbon targets were polished, and the surface roughness was measured with an atomic force microscope to be less than 25 Å. The target could be observed with a microscope under operation of the laser with and without short pulse injection. Without short pulse injection from the DFDL, no signs of plasma formation could be observed when the ASE from both amplifiers was focused on the target. When the frequency doubled, the background-free DFDL pulse amplified, a bright spot accompanied by a plasma jet appeared.

The prepulse sensitivity of the targets was also tested in an independent experiment, in which a standard KrF laser with a 20 ns pulse width was focused on the target surface. Faint signs of plasma formation appeared at an intensity of 8×10^7 W cm^{-2} on the target. This is still a factor of 2 higher than the ASE intensity under the most unfavorable conditions and an order of magnitude higher than the ASE pedestal for typical conditions of $I=10^{17}$ W cm^{-2}.

The reflected laser radiation from the carbon and aluminum targets was measured in the specular direction by a calorimeter whose acceptance aperture was four times larger than the reflected beam. Investigation of the scattered beam profile at this position indicated, however, that the laser was scattered, essentially in the specular direction, in agreement with earlier observations at lower intensities and similar pulse lengths.[5,10]

The spectra of the x rays emitted from the carbon targets were measured by a grazing incidence spectrometer in the wavelength range between 25 ($\sim$500 eV) and 250 Å ($\sim$50 eV).[3] The spectrum showed H-like and He-like carbon lines, but was dominated in energy by a broad continuum that extended beyond the short wavelength cutoff of the spectrometer. The x-ray yield measurements from aluminum and carbon targets were obtained using a Schottky type GaAsP photodiode behind a 1.6 μm thick Al filter. The filter consisted of two foils, each coated with 0.8 μm aluminum layers in order to avoid radiation leakage

through microscopic pinholes. This detector–filter combination is sensitive for photon energies exceeding $E=0.5$ keV, with a slowly decreasing sensitivity for $E>4$ keV.[25] The x-ray detector viewed the target surface under an angle of 25° from normal.

A fast x-ray streak camera also equipped with a 2 μm aluminum filter was used to measure the temporal duration of the x-ray emission. For an aluminum target irradiated at an angle of incidence of $\alpha=45°$ with p-polarized light at an intensity of $I_0=2\times10^{16}$ W cm^{-2}, the temporal duration of the x-ray emission for $E>0.5$ keV is below the 2 ps temporal resolution of the camera, in agreement with earlier experiments using visible laser wavelengths and other target materials.[5]

The radiation that was backscattered from the carbon target was observed with a vacuum ultraviolet (VUV) spectrometer, which was sensitive between 70 and 550 nm. A photomultiplier equipped with a sodium–salycilate scintillator served as a detector. The signals were strong enough that the spectrometer was almost always operated near its resolution limit of 0.2 nm. The signal was analyzed in a boxcar integrator and plotted.

Experiments measuring emission from the laser irradiated glassy carbon targets between 70 and 550 nm were performed for normal incidence of the laser on the target and observation under 45° at an intensity of 3×10^{17} W cm^{-2}. A large number of emission lines were found in the entire range from vacuum ultraviolet to the visible. The most intense lines were assigned to carbon transitions of varying ionization stages. No intense lines due to other elements could be identified. The line spectrum was dominated by the scattered fundamental of the KrF at 248 nm and the second harmonic at 124 nm. No signal at the third harmonic at 83 nm or at higher harmonic wavelengths was detected for perpendicular incidence of the beam and observation under 45°. Furthermore, no evidence was found for Raman signals at $\frac{3}{2}$ or $\frac{1}{2}$ of the fundamental laser frequency corresponding to wavelengths of 165.5 and 497 nm. This indicates a steep plasma density gradient, which is expected for a clean ultrashort laser pulse.

III. EXPERIMENTAL RESULTS

A. Absorption

The reflectivity from both aluminum and glassy carbon targets for a constant angle of incidence of 45° and s and p polarization in the intensity range of 10^{11} W cm^{-2} to 2×10^{17} W cm^{-2} is shown in Fig. 2. Reflectivity measurements from several previous investigations using ultraviolet laser radiation have also been included in this figure. Milchberg *et al.*[8] have investigated the intensity range from 10^{11}–10^{15} W cm^{-2}. Fedosejevs *et al.*[10] have obtained reflectivity data at 10^{14}–3×10^{15} W cm^{-2} for $\alpha=45°$ and 10^{12}–10^{14} W cm^{-2} for perpendicular incidence. Within experimental errors, it is evident that for high intensities the reflectivity is the same for aluminum and glassy carbon, and almost constant between 10^{15} and 10^{17} W cm^{-2}. The difference in s- and p-polarization persists up to intensities in excess of 10^{17} W cm^{-2}. The collisional absorption component $A_c=1-R_s$, where R_s is the reflectivity for s-polarized light at a 45° angle of incidence, appears to decrease slightly from $A_c=0.4\pm0.1$ at 10^{15} W cm^{-2} to $A_c=0.3\pm0.1$ at 10^{17} W cm^{-2}. Since the reflectivity for p-polarized light R_p stays approximately constant at $R_p\approx0.3$, the noncollisional absorption component $A_{nc}=R_s-R_p$ is on the order of $A_{nc}=0.3\pm0.1$, with a possible slight increase for increasing intensity.

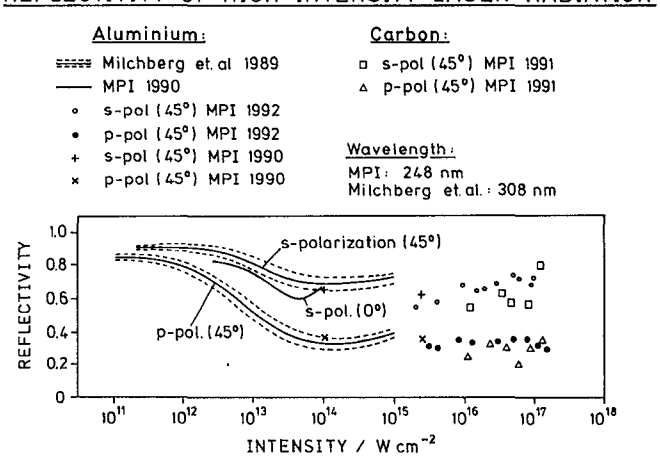

FIG. 2. Reflectivity of femtosecond KrF laser pulses from aluminum and carbon targets as functions of intensity.

The reflected laser energy and the x-ray yield were measured for s- and p-polarized KrF laser radiation as a function of intensity on an aluminum target for three different angles of incidence. The result of this experiment is shown in Fig. 3. For each angle of incidence and both polarizations, the reflectivity $R(\alpha,I_0)$ shows a very weak increase with increasing intensity. In each case the reflectivity is significantly higher for s-polarized than for p-polarized light. For p-polarized laser light, the maximum total absorption $A_p=1-R_p$ of the laser radiation in the plasma exceeds $A_p=0.7$, even at an intensity above 10^{16} W cm^{-2}. For $\alpha=45°$ and 5×10^{15} W cm$^{-2}<I_0<5\times10^{16}$ W cm^{-2}, the difference in absorption between p- and s-polarized light is constant at about $A_p-A_s=0.3$.

B. X-ray emission

For all angles of incidence, the spectrally integrated x-ray emission increases strongly with increasing intensity. Within the experimental errors, the intensity scaling of the x-ray signal X is, however, independent of the angle of incidence α and the polarization of the laser light. For the absorbed intensity I_{abs}, a power law dependence of $X\approx I_{abs}^{\gamma}$ with $\gamma=2.2\pm0.2$ is obtained from the experimental data for 10^{15} W cm$^{-2}<I_{abs}<5\times10^{16}$ W cm^{-2}.[6]

Figure 4 shows the x-ray signal ratio for s- and p-polarized pump light as a function of the angle of incidence. The upper curve corresponds to a constant laser intensity. The relative increase of the x-ray yield for p-polarized over s-polarized light has a distinct maximum at intermediate angles of $\alpha\approx45°$. For this angle,

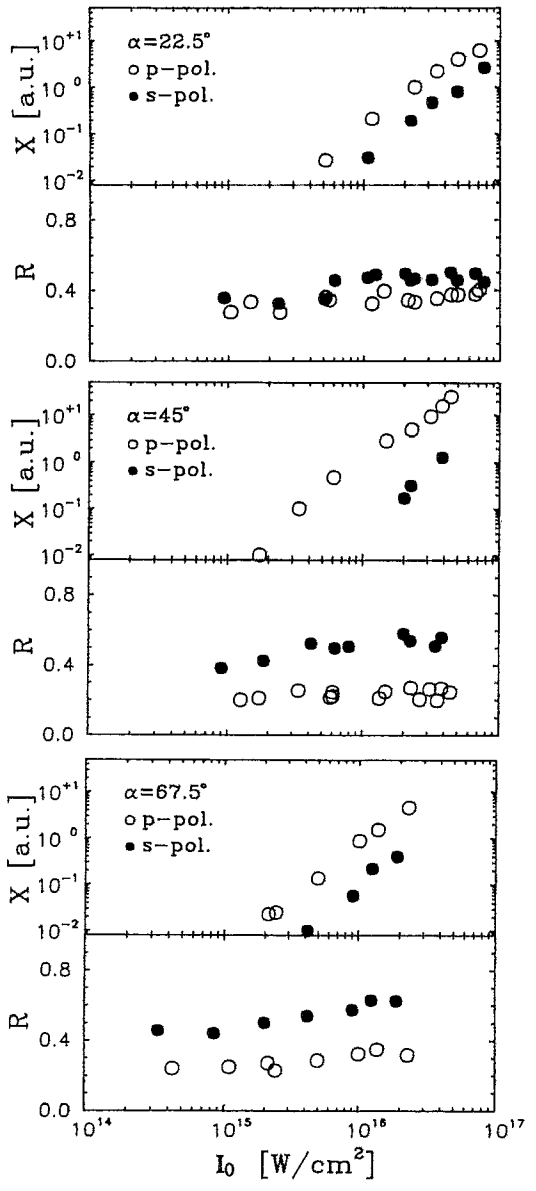

FIG. 3. Reflectivity R and integrated x-ray emission X from a polished aluminum target as a function of input intensity I_0 of a 350 fs KrF (248 nm) laser for s- and p-polarized light and three angles of incidence α. The experimental data are averaged over 25 shots. The size of the symbols indicates the statistical error. The relative systematic error is estimated to be less than 10% for the reflectivity measurements.

p-polarized light produces 15 times more x rays than s-polarized light at the same input intensity. When the experimentally determined angle- and polarization-dependent reflectivities are taken into account, the ratio of x-ray emission for s- and p-polarization can be obtained as a function of the absorbed intensity. The lower curve in Fig. 4 shows that for *constant absorbed* intensity p-polarized pump light incident under $\alpha=45°$ is still a factor of 5 more efficient in producing x rays than s-polarized light.

C. Reflected laser spectra

The spectral line shape and the positions of the reflected fundamental from the carbon plasma showed a substantial intensity dependence. The spectral width of the unscattered laser spectrum [Fig. 5(a)] of $\Delta_L=0.7$ nm is partially caused by a chirp on the laser pulse. The chirp of the laser is assumed to be partially linear, since 350 fs pulses can be compressed by a prismatic compressor to about 200 fs.[26] Figures 5(b) and 5(c) show spectra of the laser fundamental backscattered from carbon targets for an angle of incidence of 22.5°, p-polarized light and observation in the direction of the specularly reflected beam. At an intensity of 10^{16} W cm^{-2} [Fig. 5(b)], the spectrum broadens to a width of 1.1 nm (FWHM) and develops a shoulder on the blue wing. It also extends considerably farther into the red than the spectrum of the unscattered laser beam. When the intensity is increased to 3.5×10^{17} W cm^{-2}, the linewidth of the backscattered laser line narrows to $\Delta_H=0.5$ nm. The spectrum is not only narrower than at the lower intensity, but also narrower than the unscattered laser spectrum. The peak positions of the scattered laser lines also vary considerably with intensity. At $I=10^{16}$ W cm^{-2}, the peak is red-shifted by about $\delta\lambda=+0.1$ nm, whereas a blue-shift of $\delta\lambda=-0.1$ nm is observed at $I=3.5\times10^{17}$ W cm^{-2}.

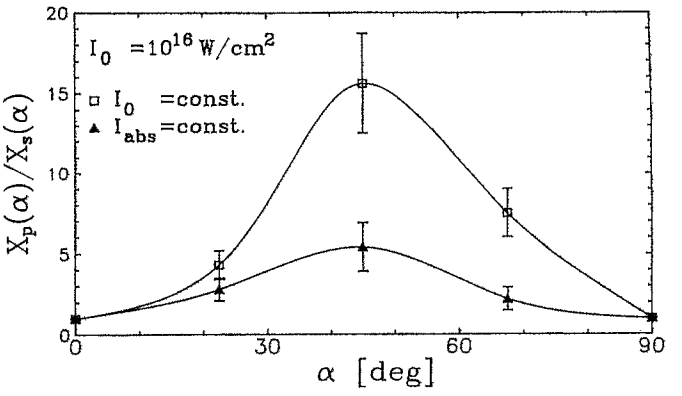

FIG. 4. Ratio of integrated x-ray emission X_p/X_s as a function of the angle of incidence for p- and s-polarized, 350 fs KrF laser irradiation. The upper curve (open squares) corresponds to constant input intensity $I_0=10^{16}$ W cm^{-2}, while the lower curve (full triangles) gives the x-ray emission ratio X_p/X_s for any constant absorbed intensity in the range of 10^{16} W cm^{-2}. At intermediate angles, the x-ray yield for p-polarized light in each case is significantly higher than for s-polarized light. The solid lines are spline interpolations through the experimental data points.

IV. MODEL OF LASER–PLASMA INTERACTION

To obtain information about the plasma from the experimentally measured reflected spectra, a one-dimensional time-dependent plasma model that includes dynamic temperature, energy balance, radiation pressure, thermal pressure, and cooling by ionization was developed. The electron density profile is approximated by a series of small discrete steps, and the optical impedance method[27] is used to calculate the reflectivity. The complex index of refraction is constant within each step, and is found from the Drude model.[8,10,11] For each step in time, the electron density and consequently the optical properties change, causing a time-dependent reflectivity. The electron–ion colli-

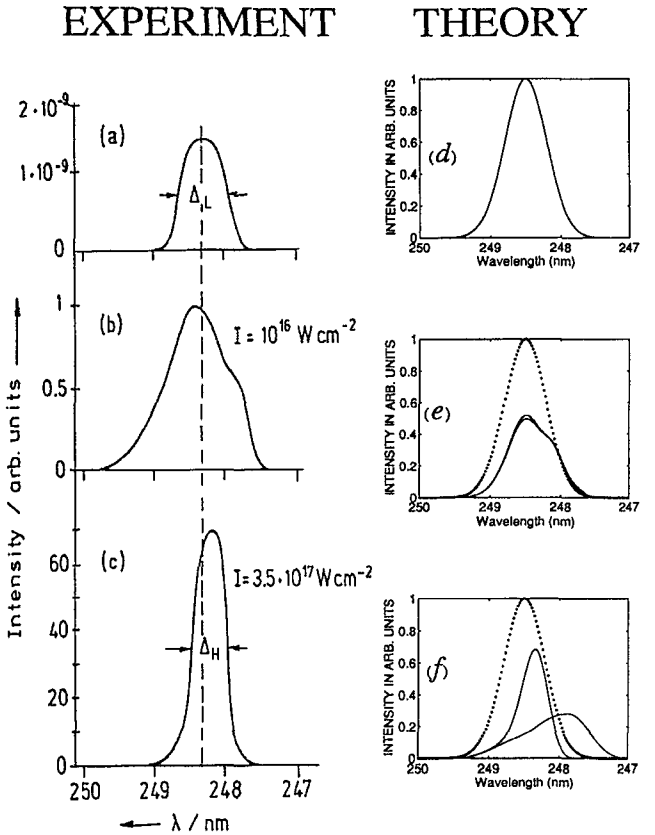

FIG. 5. Experimental and calculated spectra from carbon targets. (a) Experimental spectrum of the incoming pulse. (b) Reflected spectrum, $I=10^{16}$ W cm^{-2}. (c) Reflected spectrum, $I=3.5\times10^{17}$ W cm^{-2}. (d) Calculated Gaussian spectrum of the incoming pulse with a temporal FWHM=350 fs, spectral FWHM=0.7 nm, and positive linear chirp of $a=2.8\times10^{-5}$ fs^{-2}. (e) Calculated spectra at $I=10^{16}$ W cm^{-2} with and without radiation pressure taken into account, where $\kappa=2$. (f) Calculated spectra at $I=3.5\times10^{17}$ W cm^{-2} with and without radiation pressure taken into account, where $\kappa=10$. The solid line with the highest peak value shows the spectrum when radiation pressure is considered.

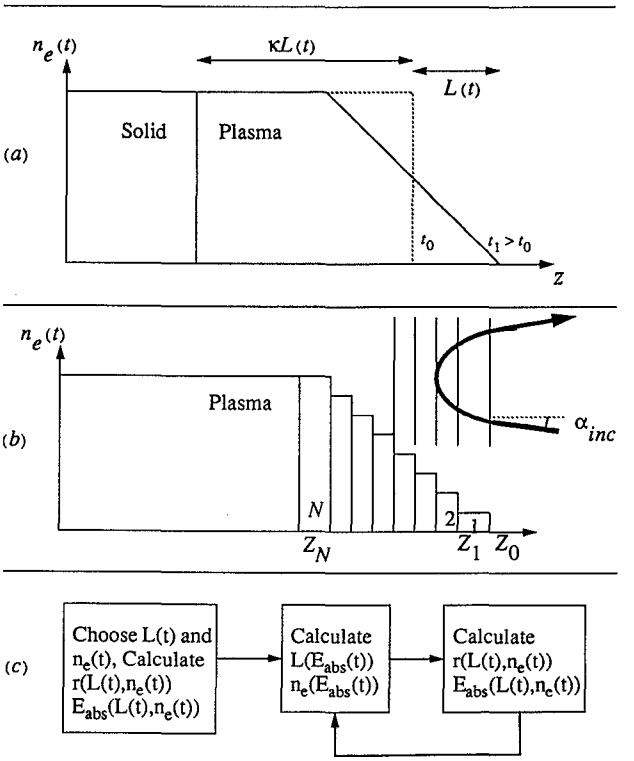

FIG. 6. (a) The plasma is modeled with a linear electron density profile expanding outward with the ion acoustic velocity minus a correction for radiation pressure. The ionization front travels into the solid with velocity κv_i. (b) Geometry for calculating the reflectivity by the optical impedance method. The curved arrow indicates the propagation of the electromagnetic wave. (c) The block diagram for the iterative plasma simulations.

sion frequency ν_{ei} is kept constant in time and space, with a value that gives reflectivities of the same magnitude as in the experiment ($\nu_{ei}=0.7\omega_{\text{Laser}}$). The electron density profile is assumed to be linear and isothermal. Despite the short time scale, the assumption of local thermal equilibrium at high densities is a good approximation, because the electron ion collision time is on the order of a few femtoseconds.[8] A one-dimensional treatment is justified, since the typical plasma expansion length $L\ll\lambda/2$ is less than 5% of the spot size.

The plasma model is schematically described in Fig. 6. As the laser pulse impinges on the target, the absorbed energy leads to rapid ionization and heating of the material. The plasma is cooled by thermal conduction while it expands. Instead of using thermal conductivity with an adjustable flux limiter in the present treatment, the absorbed laser energy is distributed among an increasing number of particles given by $N = Z(t)n_{e_{\text{solid}}}L(t)\kappa$, with κ replacing the flux limiter. Here $n_{e_{\text{solid}}}$ is the electron density corresponding to singly ionized solid density carbon, $Z(t)$ is the ionization stage, $L(t)$ is the integral of the ion acoustic velocity, $v_i(t)=[Z(t)kT_e/M_i]^{1/2}$, with respect to time and corresponds to the scale length, and $\kappa v_i(t)$ is the velocity of the ionization front propagating into the solid. Here κ is chosen, such that the simulations give agreement with experimentally determined temperatures.[8,19] In addition, $Z(t)$ is calculated from the absorbed energy. Ionization is included in the model and reduces the plasma temperature. The electron density and temperature as a function of absorbed energy are found by solving the Saha equation for the solid density carbon plasma. Figure 6(b) shows the geometry for the calculation of reflectivity. The curved arrow represents the incoming electromagnetic wave traveling through the plasma, being deflected at the turning point where $n_e=\cos^2(\alpha)n_{ec}$, $n_{ec}=1.8\times10^{22}$ cm^{-3} is the critical plasma density at the KrF wavelength.

Figure 6(c) shows a block diagram for the calculation of time-dependent reflectivity. We start with an estimate for the temporal evolution of the electron density profile, which is used to calculate reflectivity and absorbed energy as a function of time. The value for the absorbed energy is then used to calculate the temporal evolution of the plasma profile, and new values for $L(t)$ and $n_e(t)$ are obtained as improved estimates. The process is repeated until it converges, typically 5–10 times for five digit accuracy. The

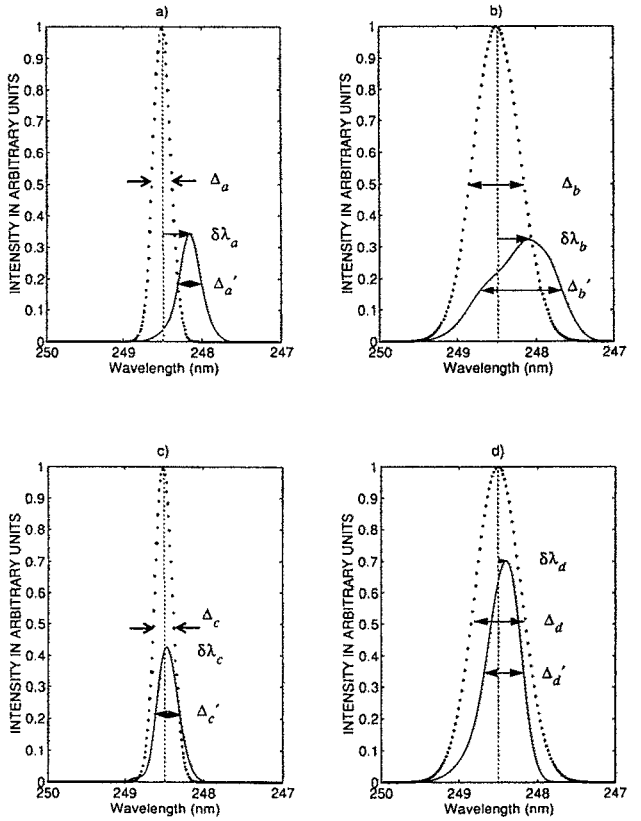

FIG. 7. Calculated spectra reflected from a carbon target irradiated by 350 fs chirped and unchirped pulses at an angle of incidence of 22.5° with p-polarized light at an intensity of 10^{17} W cm^{-2}. In each panel, the dotted line shows the incoming pulse spectrum. (a) Reflected spectrum from a plasma produced by an unchirped incoming pulse when radiation pressure is ignored. (b) Reflected spectrum from an incoming pulse with linear chirp $a=2.8\times10^{-5}$ fs^{-2} when radiation pressure is ignored. (c) Reflected spectrum from an unchirped incoming pulse when radiation pressure is included in the simulation. (d) Reflected spectrum from an incoming pulse with linear chirp $a=2.8\times10^{-5}$ fs^{-2} when radiation pressure is included.

evolution of the profile is defined by the integral of the ion acoustic velocity reduced by a correction found by integrating the acceleration of the reflective surface due to radiation pressure. The reflected electric field is obtained by multiplying the incoming electric field by the complex reflection coefficient. The backscattered spectrum is then found by taking the absolute square of the Fourier transform of the reflected complex electric field.

The model is applied to a carbon target irradiated at an angle of incidence of 22.5° with p-polarized light at an intensity of 10^{17} W cm^{-2}, and the reflected spectra are shown for both chirped and unchirped incoming pulses. Figures 7(a) and 7(b) show spectra of the reflected radiation when the radiation pressure is ignored and the plasma expands with the ion acoustic velocity. The dotted line represents the spectrum of the unscattered fundamental throughout Fig. 7. In each case the incident laser pulse has a Gaussian pulse shape. In Fig. 7(a), the incoming pulse has a pulse duration of 350 fs and is bandwidth limited. The blue shift ($\delta\lambda$) amounts to $\delta\lambda_a=-0.35$ nm, while the spectral width increases from $\Delta_a=0.27$ nm to $\Delta_a'=0.32$ nm. Figure 7(b) shows the spectrum of the backscattered fundamental when the incoming pulse has a positive linear chirp of $a=2.8\times10^{-5}$ fs^{-2} and a spectral width of $\Delta_b=0.7$ nm (FWHM). The reflected pulse is broadened to $\Delta_b'=1.0$ nm and $\delta\lambda_b=-0.4$ nm.

When the radiation pressure is included, the velocity of the reflective surface is a superposition of the ion acoustic velocity and the motion of the inertial mass of the reflective surface when the force per unit area is $\cos(\alpha)[1+R(t)]I(t)/c$, where α is the angle of incidence, $R(t)$ is the reflectivity, $I(t)$ is the intensity envelope of incoming pulse, and c is the velocity of light in vacuum. An estimate for the inertial mass of the reflective surface is the mass of the ions contained within one skin depth of the critical density. This estimate was used for the simulations.

For an intensity of 10^{17} W cm^{-2}, the effects of the radiation pressure are very important. Figure 7(c) shows the reflected spectrum for an unchirped pulse, for which $\delta\lambda_c=-0.03$ nm and $\Delta_c'=0.32$ nm. For a chirped pulse with the same parameters as in Fig. 7(b), Fig. 7(d) shows that the spectral width changes from $\Delta_d=0.7$ nm to $\Delta_d'=0.5$ nm, whereas $\delta\lambda_d=-0.10$ nm. Although Figs. 7(c) and 7(d) represent exactly the same plasma condition for chirped and unchirped pulses, the peak wavelength shifts differ by a factor of 3. These calculations suggest that the formula $\delta\lambda/\lambda=2\cos(\theta)v/c$ for Doppler shifts is valid only for bandwidth limited pulses, where v applies to the time-averaged velocity.

V. DISCUSSION

The reflection experiments show that the absorption of ultrashort pulse high-intensity ultraviolet laser radiation in the intensity range between 10^{15} and 10^{16} W cm^{-2} (Figs. 2 and 3) is significantly higher than for a 1 ps, 1 μm laser light.[9] The absorption at 10^{15} W cm^{-2} is comparable to that given by Milchberg *et al.*,[8] using an aluminum target and the same angle of incidence, but a laser wavelength of 308 nm, and that obtained by Fedosejevs *et al.*[10] for 248 nm (Fig. 2).

Most interesting is the much higher efficiency for x-ray generation by p-polarized KrF laser light as compared to that for s-polarized light for constant absorbed intensity (Fig. 4). If the absorption of the laser radiation were due to collisional absorption only, the x-ray signal would be expected to be a function of the absorbed intensity only and independent of the angle of incidence and polarization for constant absorption. Since this is not observed (Fig. 4), noncollisional, angle and polarization-dependent absorption processes, such as resonance absorption or vacuum heating, must contribute to the total absorption.[6] Resonance absorption has also recently been cited as the cause for enhanced absorption of intense short pulse laser radiation in porous targets.[28]

For laser plasmas with scale lengths L larger than or equal to the laser wavelength ($L/\lambda\geqslant1$), resonance absorption is theoretically well understood,[29] and a strongly angle-dependent absorption with a maximal value of

$A_{nc} \approx 0.5$ for p-polarized light is predicted. The other extreme of very short plasma scale length ($L/\lambda \ll 1$) is described by the Drude free-electron model for an overdense plasma.[30]

It is generally assumed that there is a monotonous transition between resonance absorption in the long scale length case and the high reflectivities obtained for the infinitely steep density gradient. There is, however, analytical[31,32] as well as recent numerical[13,33] evidence that this may not be the case. For small but finite scale length $L/\lambda \approx 0.1$, the thin plasma layer in front of the overdense approximately solid density plasma can act as a very efficient absorber, with absorptions up to $A \approx 1$ for p-polarized light. For the present experiments, the scale length can be estimated to be about $L \approx 50$ nm $= 0.2\ \lambda$,[6] which would satisfy the condition for high absorption formulated in Refs. 31 and 32. Since the scale length is largely determined by the plasma temperature and the laser pulse width, the total plasma absorption would be expected to depend not only on the laser intensity, but also on the laser wavelength and the pulse duration, even in the subpicosecond regime. Although this might qualitatively explain some of the differences between different absorption measurements, much more detailed comparisons between well-controlled experiments and theory are necessary.

In the following, the predictions of the laser–plasma interaction model (Sec. IV) are compared to the experimental results for the backscattered laser pulse. Figures 5(e) and 5(f) show the resulting spectra from simulating the experimental conditions under which the reflected pulse spectra of Figs. 5(b) and 5(c) were measured. When the incoming intensity is 10^{16} W cm^{-2}, the experimental and simulated spectrum have similar shape, but the experimental spectrum is broader than what the model predicts, 1.1 nm vs 0.8 nm (FWHM). For an incoming intensity 3.5×10^{17} W cm^{-2}, the simulation in Fig. 5(f) closely matches the experimental result both for a change in spectral width and blue shift. Both the model and experimental results show that the lower intensity makes the reflected spectrum broader, whereas the higher intensity narrows the reflected spectrum.

For an intensity of $I = 3.5 \times 10^{17}$ W cm^{-2}, the model gives is a plasma expansion velocity that varies between 0 and 1.8×10^5 ms^{-1} during the incoming pulse, with a substantial deceleration due to the radiation pressure near the peak of the pulse. The deceleration of the critical density surface results in a phase shift with negative second temporal derivative, reducing the chirp of the reflected pulse. Therefore, the spectral FWHM of the reflected laser pulse is smaller than that of the incoming pulse.

The reflected spectrum shown in Fig. 5(b) results from a plasma in which the reflective surface accelerates and the absorption increases during the time span of the incoming pulse. The acceleration of the reflective surface causes spectral broadening, while the time-dependent absorption of the incoming chirped pulse causes the red shift. Because the "reddest" component precedes the "bluest" component of the chirped pulse, a reflectivity that decreases with time effectively acts as a filter discriminating against the shortest wavelengths, and this causes the red shift.

Both the experimental results (Fig. 5) and the plasma simulations (Figs. 5 and 7) show that the spectra of the backscattered radiation depend on, at least, two effects. First, the plasma expansion causes spectral shifts (Doppler shift) and chirp is added to the reflected spectrum during the acceleration. The chirp can be positive or negative, depending on the relative magnitudes of the radiation pressure and the plasma pressure, which are both functions of time. Second, the electron density and, consequently, the optical properties of the plasma that determine the absorption, change during the pulse. This changes the temporal and spectral pulse shape. For a chirped pulse where the instantaneous frequency of the laser pulse changes in time, a plasma with a time-dependent reflectivity can act as a frequency filter, adding to or subtracting from the Doppler shift.

VI. CONCLUSIONS

The simple time-dependent model presented in this paper qualitatively describes how time-dependent plasma parameters at high intensities cause spectral modifications of the backscattered laser pulse. Because the spectral shifts and line shape changes result from the combined effect of Doppler shifts and self-phase modulation, the interpretation of such spectra becomes difficult, and the extraction of even temporally averaged plasma expansion velocities has to be performed with great care. With ever increasing laser intensities, the regime of small but finite scale length is expected to be of increasing importance. Experiments show that even well-controlled 100 fs (FWHM) laser pulses of intensities in the range of $\sim 10^{18}$ W cm^{-2} have pulse widths exceeding 1 ps at the 10^{14} W cm^{-2} level.[34] Therefore, even "clean" pulses will generate an underdense plasma of short scale length on the order of $L/\lambda \approx 0.1$. Since high absorption can be obtained under those conditions, this regime might prove fruitful in future x-ray generation experiments.

ACKNOWLEDGMENTS

It is a pleasure to thank S. Szamari, P. Simon, and J. Bergmann for their help with the laser system.

This work was supported by the Bundesministerium für Forschung und Technologie (BMFT). R. S. has profited from discussions at a CECAM workshop and acknowledges support from the Humboldt Foundation and the National Science Foundation.

[1] J. D. Kmetec, C. L. Gordon, J. J. Macklin, B. E. Lemoff, S. G. Brown, and S. E. Harris, Phys. Rev. Lett. **68**, 1527 (1992).
[2] J. A. Cobble, G. A. Kyrala, A. A. Hauer, A. J. Taylor, C. C. Gomez, N. D. Delameter, and G. T. Schappert, Phys. Rev. A **39**, 454 (1989); also, G. A. Kyrala, R. D. Fulton, E. Wahlin, L. A. Jones, G. T. Schappert, J. A. Cobble, and A. J. Taylor, Appl. Phys. Lett. **60**, 2195 (1992).
[3] U. Teubner, G. Kühnle, and F. P. Schäfer, Appl. Phys. Lett. **59**, 2672 (1991); Appl. Phys. B **54**, 493 (1092).
[4] D. G. Stearns, O. L. Landen, E. M. Campbell, and J. H. Scofield, Phys. Rev. A **37**, 1684 (1988).

[5]M. M. Murnane, H. C. Kapteyn, M. D. Rosen, and R. W. Falcone, Science **251**, 531 (1991); M. M. Murnane, H. C. Kapteyn, and R. W. Falcone, Phys. Rev. Lett. **62**, 155 (1989).
[6]U. Teubner, J. Bergman, B. van Wonterghem, F. P. Schäfer, and R. Sauerbrey, Phys. Rev. Lett. **70**, 794 (1993).
[7]H. Chen, B. Soom, B. Yaakobi, S. Uchida, and D. D. Meyerhofer, Phys. Rev. Lett. **70**, 3431 (1993).
[8]H. M. Milchberg, R. R. Freeman, S. C. Davey, and R. M. More, Phys. Rev. Lett. **61**, 2364 (1988); H. M. Milchberg and R. R. Freeman, J. Opt. Soc. Am. B **6**, 1351 (1989).
[9]J. C. Kieffer, P. Audebert, M. Chaker, H. Pépin, T. W. Johnston, P. Maine, D. Meyerhofer, J. Delettrez, D. Strickland, P. Bado, and G. Mourou, Phys. Rev. Lett. **62**, 760 (1989).
[10]R. Fedosejevs, R. Ottmann, R. Sigel, G. Kuhnle, S. Szatmari, and F. P. Schäfer, Phys. Rev. Lett. **64**, 1250 (1990); R. Fedosejevs, R. Ottmann, R. Sigel, G. Kuhnle, S. Szatmari, and F. P. Schäfer, Appl. Phys. B **50**, 79 (1990).
[11]S. C. Rae and K. Burnett, Phys. Rev. A **44**, 3835 (1991).
[12]O. L. Landen and W. E. Alley, Phys. Rev. A **46**, 5089 (1992).
[13]J-C. Kieffer, J-P. Matte, S. Bélair, M. Chaker, P. Audebert, H. Pépin, P. Maine, D. Strickland, P. Bado, and G. Mourou, IEEE J. Quantum Electron. **QE-25**, 2640 (1989).
[14]H. M. Milchberg and R. R. Freeman, Phys. Fluids B **2**, 1395 (1990); H. M. Milchberg and R. R. Freeman, Phys. Rev. A **41**, 2211 (1990).
[15]D. Umstadter, X. Liu, J. S. Coe, and C. Y. Chien, in *OSA Proceedings on Short-Wavelength Coherent Radiation*, edited by P. H. Bucksbaum and N. M. Ceglio (Optical Society of America, Washington, DC, 1991), Vol. 11, pp. 276–280.
[16]R. Dübgen and G. Popp, Z. Werkstofftechnik **15**, 331 (1984) (in German).
[17]S. Szatmari and F. P. Schäfer, Opt. Commun. **68**, 196 (1988).
[18]G. Almasi, S. Szatmari, and P. Simon, Opt. Commun. **88**, 231 (1992).
[19]A. Ziegler, P. G. Burkhalter, D. J. Nagel, M. D. Rosen, K. Boyer, G. Gibson, T. S. Luk, A. McPherson, and C. K. Rhodes, Appl. Phys. Lett. **59**, 534 (1991).
[20]D. Kühlke, U. Herpers, and D. von der Linde, Appl. Phys. Lett. **50**, 1785 (1987).
[21]H. W. K. Tom and O. R. Wood, Appl. Phys. Lett. **54**, 517 (1989).
[22]S. E. Harris and J. D. Kmetec, Phys. Rev. Lett. **61**, 62 (1988).
[23]F. P. Schäfer, J. Phys. Coll. C6, Suppl. 10 **47**, 149 (1986).
[24]J. A. Cobble, G. T. Schappert, L. A. Jones, A. J. Taylor, G. A. Kyrala, and R. D. Fulton, J. Appl. Phys. **69**, 3369 (1991).
[25]M. Krumrey, E. Tegeler, J. Barth, M. Krisch, F. Schafers, and R. Wolf, Appl. Opt. **27**, 4336 (1988); D. Y. Smith, E. Shiles, and M. Inokuti, in *Handbook of the Optical Constants of Solids*, edited by E. D. Palik (Academic, London, 1985).
[26]S. P. Le Blanc, F. Cote, G. Szabo, and R. Sauerbrey, in *Ultrafast Pulse Generation and Spectroscopy*, edited by T. R. Gosnell, A. J. Taylor, K. A. Nelson, and M. C. Downer (Society of Photo-optical Instrumentation Engineers, Bellingham, WA, 1993), Vol. 1861, pp. 161–169.
[27]L. M. Brekovskikh, *Waves in Layered Media* (Academic, Orlando, 1960).
[28]S. P. Gordon, R. Sheppard, T. Donnelly, D. Price, B. White, A. Osterheld, H. Hamster, A. Sullivan, and R. W. Falcone, in *Short Wavelength V: Physics with Intense Laser Pulses* (Optical Society of America, Washington, DC, 1993), Vol. 17, pp. 203–205.
[29]W. L. Kruer, *The Physics of Laser Plasma Interaction* (Addison–Wesley, New York, 1988); V. L. Ginsburg, *The Propagation of Electromagnetic Waves in Plasmas* (Pergamon, New York, 1970).
[30]R. M. More, Z. Zinaman, K. H. Warren, R. W. Falcone, and M. Murnane, J. Phys. Coll. C7, Suppl. 12, **49**, 43 (1988).
[31]R. P. Godwin, Phys. Rev. Lett. **28**, 85 (1972).
[32]H. J. Kull, Phys. Fluids **26**, 1881 (1983).
[33]P. Gibbon and A. R. Bell, Phys. Rev. Lett. **68**, 1535 (1992).
[34]C. Rouyer, E. Mazataud, I. Allais, A. Pierre, R. Rossage, S. Seznec, C. Sauteret, A. Migus, and G. Mourou, in *Short Wavelength V: Physics with Intense Laser Pulses* (Optical Society of America, Washington, DC, 1993), Vol. 17, pp. 2–5.